Pilot-Vehicle Analysis of Multiaxis Tasks

Duane McRuer*
Systems Technology, Inc., Hawthorne, California
and
David K. Schmidt†
Purdue University, West Lafayette, Indiana

In missions where high cognitive and managerial requirements are placed on the pilot, or where failures may significantly degrade one or more aircraft control axes, the pilot must divide his attention among several tasks. The pilot and system behavior in such divided-attention conditions, and the combination of pilot ratings from single to multiaxis conditions are treated using classical and optimal control models for the human in a complementary fashion. It is shown that the crossover frequency and closed-loop system performance for a given axis under divided attention will be less than full-attention values, while the remnant and the phase margin will be greater, and that the model-based trends are consistent with experiment. Also, the optimal control performance index used in the pilot and system behavioral modeling, when "calibrated" with single-axis correlations, shows potential for the development of subjective rating estimates for multiaxis tasks.

Introduction

THE pilot of a modern high-performance aircraft must perform both control and managerial functions in most mission phases. In some, such as final approach and landing or a variety of air-to-air or air-to-ground tracking tasks, the control function is paramount and requires most of the pilot's available attention. In the past the more difficult of these control tasks have tended to expose whatever unfavorable effective aircraft dynamic (flying quality) problems were present. Consequently, pilot modeling for the consideration of critical flying qualities has tended to be focused on full-attention or nearly full-attention control operations. Further, the vast majority of pilot dynamics and pilot rating data used to develop flying quality boundaries have been obtained for situations where the dynamic properties of one control axis are varied, while maintaining the dynamics of other axes at "good" levels.

With modern missions in which high cognitive and managerial requirements are placed on the pilot, or where failures may significantly degrade one or more aircraft control axes, the pilot must divide his attention among several axes or, more generally, between control and other tasks. In such situations the vehicle dynamics in each axis being controlled by the pilot must be superior to those that would be suitable if the pilot could devote almost full attention to just one axis.

This state of affairs brings two key issues to the fore. The first is pilot and system behavior in divided-attention or task-interference situations, where several tasks compete for the pilot's attention. Critical questions in these situations relate to the standards that should be set for both desirable and minimum flying quality levels in a given axis when these standards are conditioned by the other control and managerial tasks at hand. The second is the subjective assessment, or rating, of effective vehicle dynamics in multiaxis control or multiple-task conditions.

Received June 29, 1987; presented as Paper 87-2538 at the AIAA Guidance, Navigation, and Control Conference, Monterey, CA, Aug. 17–19, 1987; revision received Sept. 13, 1988.

*President and Technical Director. Fellow AIAA.
†Professor, School of Aeronautics and Astronautics; currently Professor of Engineering, Arizona State University, Tempe, AZ.

This paper will treat both of these issues for multiaxis control tasks. It begins with a review of pilot modeling for divided-attention conditions, developing the differences to be expected in pilot and pilot-vehicle system behavior of single-axis (full-attention) and multiaxis control tasks. The major data source for which pilot ratings for both single and multiaxes are available is then used as a basis for obtaining estimates of pilot and system behavior data. These estimates are obtained using an optimal control model and serve as surrogates for pilot dynamic behavior characteristics that were not measured during the original experiments. The results from the optimal control model analysis are compared with those from classical theory and with the limited experimental evidence available. The estimation of pilot ratings is then treated using an extension of previously available correlations. Important features in these developments are the complementary connections of classical theory and optimal control modeling techniques.

Divided-Attention and Task-Interference Modeling

The classical theory of pilot-vehicle system dynamics is based on the well-known "crossover model" (see, for example, Ref. 1). In this theory the human pilot's behavior is characterized in mathematical terms as a random-input describing function Y_p, plus pilot-induced "noise" expressed as a power spectral density Φ_{nn}, commonly referred to as "remnant." In a specified task with the effective vehicle dynamics described by the transfer function Y_c, the crossover model open-loop describing function G takes the form (valid at frequencies near ω_c) shown in Fig. 1. This form is established by appropriate adjustment of Y_p by the pilot.

In the crossover model there are three key variables—the crossover frequency ω_c, the effective system latency τ, and the remnant power spectral density Φ_{nn}. The crossover frequency is sometimes loosely referred to as the pilot-vehicle system "bandwidth." It has the usual feedback system physical interpretation as the metric that divides the world of the control system into two frequency regimes: below ω_c the benefits of feedback are present (e.g., output follows input, error is reduced, etc.), whereas above ω_c the system becomes essentially open loop. The system latency theoretically appears as a pure time delay, although it is actually a low-frequency approximation to all the high-frequency (i.e., well above ω_c) net lags and delays in the system. It includes time delays and neuromuscular lags contributed by the pilot as well as net lags from

manipulators and other manual controller elements, higher frequency effective aircraft dynamics, etc. The effective aircraft dynamics include aircraft plus stability augmentation plus display, etc., dynamics. By using the effective system latency as a normalizing variable, the crossover model dynamic properties can be given in more general terms as either a normalized crossover frequency $\tau\omega_c$, or a phase margin $\phi_M = \pi/2 - \tau\omega_c$.

The remnant power spectral density depends on the amount of pilot-generated lead required to make good the crossover model form, the nature of the manipulator, and other features of the system and task. It arises primarily from fluctuations of attention and other time variations internal to the pilot.[1] When, as is usually the case, these time variations are random the power spectral density is continuous and, more important, the remnant spectral density will scale with the mean-square error.[1-4] This is depicted in Fig. 1 by the dotted line introducing $\overline{e^2}$ into the remnant block.

When the pilot's full attention is focused on a single-axis control task, the crossover frequency of the pilot-vehicle system is maximized, and the remnant has a minimum value that is dependent on the details (pilot-lead, manipulator characteristics, etc.) of the particular task. When more than one axis is to be controlled, or when managerial tasks are present, or when both multiaxis control and managerial operations are to be accomplished, the pilot must share his attention among the several tasks. In these cases the crossover model will still hold for the control activities, but with some modifications. The possible nature of the changes is partially exhibited in Fig. 1 by the presence of a perceptual describing function Y_h, an accompanying additional latency τ_h, and a more general name ("perceptual scanning") for the divided-attention or task-interference remnant to account for the divided attention.

Divided-attention operations can be considered as an extension to the well-established theory of display scanning and signal sampling/reconstruction.[1,3,5,6] The most important and fundamental model change is the remnant. A theoretical model for remnant due to quasirandom task switching/sampling with a constant average dwell time on the task at hand T_d, and a sampling/switching interval among tasks varying about some mean value T_s, was derived by Clement[3] and validated for visual inputs.[6] This remnant form is

$$\Phi_{nn}(\omega) = \frac{T_s\overline{e^2}\,(1-\eta)(1-\delta)}{\pi\left[1+\left(\frac{\omega T_d}{2}\right)^2\right]}\left(\frac{\text{units}^2}{\text{rad/s}}\right) \qquad (1)$$

where

$\overline{e^2}$ = mean square of the signal sampled
T_s = mean sampling interval
η = effective control dwell fraction, $= T_d/T_s$
T_d = effective dwell interval on the control task considered
δ = normalized lower bound on the domain of T_s: $T_0/T_s < 1$

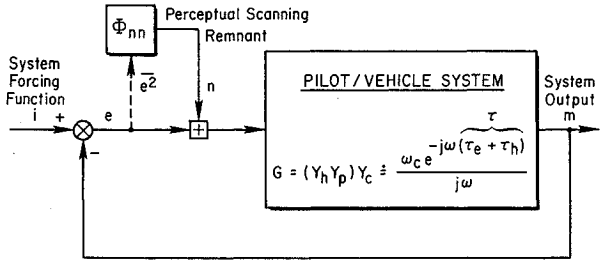

Y_c = Effective dynamics of vehicle (e.g.,aircraft plus stability augmentation plus displays)

Y_p = Full attention pilot describing function

Y_h = Perceptual describing function to account for divided attention

Fig. 1 Pilot-vehicle system for divided-attention control tasks.

Table 1 Typical values for divided-attention remnant quantities

Item	Nominal	Range
$\delta = T_0/T_s$	1/2	1/3-2/3
Minimum T_d (s)	0.4-0.5	
T_d for velocity detection (s)	0.6-0.7	
T_d for acceleration detection (s)	1.0	

This power spectrum is valid at frequencies well above the low-pass breakpoint $2/T_d$ defined by the control dwell time. The variability of the switching interval is not purely random, but is subject to a lower bound T_0. This is represented in Eq. (1) by the term $1-\delta$. The numerical values in Table 1, based on the Ref. 6 experiments involving the visual modalities and attention switches between displays, provide some appreciation for the magnitudes of some of the quantities in Eq. (1).

The major remnant variations are with the control dwell fraction η and the mean-square input to the pilot (shown as mean-square error $\overline{e^2}$ in Fig. 1). Perceptual scanning remnant is reduced by increasing the dwell fraction, going to zero when the divided-attention control task becomes full attention. [In this limiting case, full-attention remnant will still be present; this is not included in Eq. (1) because the perceptual scanning remnant is typically much larger for the divided-attention conditions of interest here. It can easily be included because the same scaling with $\overline{e^2}$, with a different proportionality factor, applies for the full-attention remnant.] Just as for the full-attention remnant, the increase of remnant power with the magnitude of the pilot's input stems from time variations, in this case the time modulation of attention inherent in the perceptual scanning process.

The implications of divided attention have been explored theoretically and experimentally for almost two decades. (The classical theory described to this point stems from Ref. 5 and includes Refs. 1 and 3-8.) A quantitative example of the effects of divided attention on task performance is presented in Fig. 2, taken from Ref. 8. Here the forcing function is "white" noise through a third-order Butterworth filter with normalized breakpoint $\omega_i\tau = 0.25$. Full attention is the lowest curve. The divided-attention conditions are then shown as a family with task dwell fraction η as the parameter. In this example, the normalized control task dwell interval is set at $T_d/\tau = 1.5$, and the divided-attention remnant normalized lower bound on the scanning interval $\delta = 0.5$.

Figure 2 illustrates the profound effects of divided attention on task performance. The perceptual scanning penalizes the performance in three important ways: 1) by a reduction of the crossover frequency (and a concomitant increase in the phase margin); 2) by an increase in the remnant; and 3) by the introduction of a new kind of "stability" constraint—"instability in the mean-square." The performance data shown in this figure indicate that, as additional tasks require more of the pilot's attention, the dwell fraction for the primary task must decrease, and the optimum operating point for the pilot shifts.

Divided-attention effects can also be modeled with optimal control models for pilot behavior. Reference 9 is an early empirical/analytical study of task interference that took this approach. In this study, the simultaneous control of several independent axes was the situation creating the task interference. From two to four axes were controlled, each with an associated display. The results were compared to single-axis control results. A model for task interference was hypothesized, and this model also focuses on remnant-related parameters. The key parameters proposed in Ref. 9 to reflect task interference are centered on the increased "measurement noise" contaminating the subject's observations of sensed quantities.

Specifically, in the optimal-control modeling approach,[10] the human is considered to observe an array of system responses, which then comprise the subject's observation vector, $\bar{y}_p(t)$. These measurements are (each) contaminated with (white) observation noise v_{y_i}, or

$$\bar{y}_p(t) = \bar{y}_{p_{\text{true}}}(t) + \bar{v}_y \tag{2}$$

Finally, the noise-intensity matrix of $\bar{v}_y$ is assumed diagonal, with elements equal to V_{ii} where i corresponds to the ith observed variable (e.g., displayed error in one axis).

For a single-axis control task and display, V_{ii} is taken to be

$$V_{ii} = P_0 \left[\frac{\sigma_{y_i}}{N(\sigma_{y_i}, T_i)}\right]^2 \tag{3}$$

where σ_{y_i} is the rms value of the response variable y_{p_i}, and $N(\sigma_{y_i}, T_i)$ is the random-input describing function of a dead zone of half-width T_i. This dead-zone model represents the effect of perception or indifference thresholds in the subjects' observations. Finally, P_0 is the nominal, full-attention noise-to-signal ratio for the observed variable y_i. This (full-attention) noise-to-signal ratio has been empirically shown to be relatively constant over a range of tasks and controlled element dynamics, and is usually taken (for foveal viewing in the case of visually sensed responses) to be approximately -20 dB (i.e., 0.01 units of normalized power per rad/s, defined over positive frequencies).[4,9] Note that this entire procedure is consistent with the "standard" optimal-control modeling approach described in Ref. 10, for example.

Now the interference model of Ref. 9 states that the effect of task interference is reflected in an increase in the effective P_0, the noise-to-signal ratio defining the observation noise intensity. With the description of task interference, the noise intensity becomes

$$V_{ii} = \frac{P_0}{f_i}\left[\frac{\sigma_{y_i}}{N(\sigma_{y_i}, T_i)}\right]^2 \tag{4}$$

where f_i is the fractional attention devoted to tasks i (or more precisely, response i), and $0 \leq f_i \leq 1$. Also, since the human's capacity is finite,

$$\sum_i f_i = 1.0$$

over all tasks and displays. This model was validated in Ref. 9 by comparing model-based tracking errors, pilot describing functions, and remnant (reflected to the displayed error) with experimental results. Because the filter dynamics, which are a portion of the pilot (model)[10] dynamics, depend on observation noises, variations in these noises manifest themselves in changes in pilot (model) dynamics and, hence, in pilot-vehicle closed-loop dynamics. (Note that in Ref. 9 the threshold effects were modeled as additional additive observation noise that did *not* scale with σ_{y_i}. The threshold effects considered in this reference were primarily due to parafoveal viewing. The use of the dead-zone describing function did not appear until after Ref. 9 was published, although its use is basically an extension of results presented in Ref. 9.)

Attention will now turn to the application of the optimal control theoretical model for task interference to the modeling of other experimental situations involving single and multiaxis tasks. These are the multiaxis experiments of Dander,[11] which are the only data set currently available in which pilot ratings are available for both single-axis and multiaxes tasks wherein the multiaxis cases involved the same dynamics as were used for the single-axis experiments. The model results will provide an "estimated pilot behavior and system performance data base," which is otherwise not available. These results can then be compared with the trends from the divided-attention theory, and also with some of the experimental results of Ref. 6.

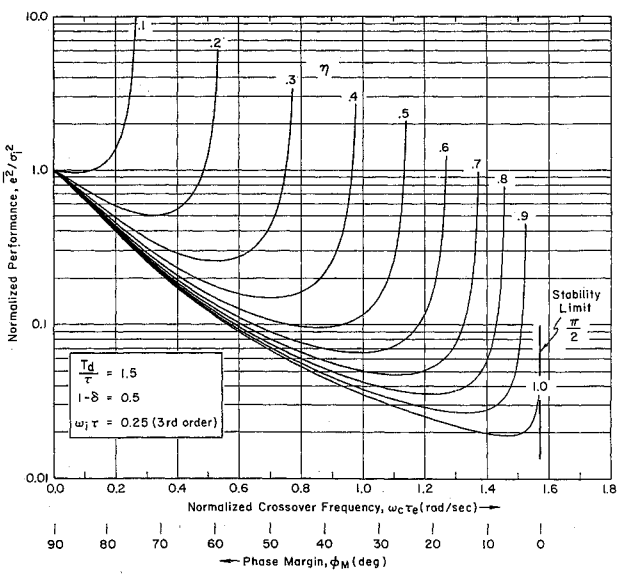

Fig. 2 Effect of divided attention on task performance.

Experimental Data

Dander[11] has reported experimental findings from single-axis and multiaxis tracking experiments. The only experimental results were in the form of subjective ratings using the Cooper scale, but both single-axis and multiaxis ratings of the same dynamics were obtained.

Dynamically independent axes were considered in the tracking experiments. Single-axis and simultaneous two- and three-axis tracking tasks were performed, and the tasks were subjectively rated. For the two- and three-axis experiments, an overall rating was given, not a rating of an individual axis in the task. Although some of the two-axis cases will be discussed here, the ratings for these cases were considered by Dander to be inconsistent with the three-axis results. This conclusion was reinforced by an independent analysis.[12] Consequently, the two-axis ratings will not be used in the analyses presented here.

Table 2 Dander controlled-element dynamics

Axis transfer functions	Good dynamics (H)	Intermediate dynamics (M)	Bad dynamics (L)
$\frac{\theta}{\delta_{E_S}} = \frac{4.(.04)(0.9)}{(1/T_\theta)(5.)(0.7,0.25)}$	$1/T_\theta = 0$	$1/T_\theta = -0.5$	$1/T_\theta = -0.8$
$\frac{\phi}{\delta_{A_S}} = \frac{0.5(0.1)}{(1.5)[\zeta_\phi, 0.5]}$	$\zeta_\phi = 0.84$	$\zeta_\phi = -0.3$	$\zeta_\phi = -0.84$
$\frac{\beta}{\delta_{Rp}} = \frac{10.(0.1)}{(3.0)[\zeta_\beta, 0.5]}$	$\zeta_\beta = 0.5$	$\zeta_\beta = -0.2$	$\zeta_\beta = -0.5$

Notations: $(s + a) \equiv (a)$; $[s^2 + 2\zeta\omega s + \omega^2] \equiv [\zeta, \omega]$.

The controlled-element dynamics in each axis were varied to obtain a wide variety of combinations of configurations. The dynamics for each axis were initially selected to yield level 1, 2, and 3 ratings in the *single-axis tracking task*. And three different dynamic elements were selected for each axis, yielding a total of nine different dynamic elements. These transfer functions are listed in Table 2.

The configurations to be considered herein, along with the ratings obtained in the Ref. 11 experiments are listed in Table 3, with configuration symbols used in later graphical presentations.

The command signals in each axis consisted of sums of sinusoids, generating random-appearing signals. The amplitudes and frequencies of the sinusoids used in each of the three command signals are listed in Table 4, along with the approximate maximum command-signal amplitude. Note that the units of displayed commands are inches of command-bar displacement on the displacement on the display θ_c, angle of rotation of the command bar ϕ_c, and "display units" (approximately 7 deg of rotation of a needle on a circular dial = 1 unit) (β_c). Also, it is noted that most of the power in the signals is in frequencies below 0.5 rad/s, with the maximum frequency in the signals equal to 1.32 rad/s.

Optimal Control Modeling of the Experiment

The modeling process now involves representing the task in terms of the parameters in the optimal control framework.[10] These include the following:

1) An appropriate objective function representative of the task (or a generic task critical to the performance of the actual task).

2) The value for the neuromotor time constant in each axis.

3) The parameters that determine the observation noise intensities: nominal noise-to-signal ratio P_0; perception/indifference threshold T_i; and attentional allocation (may be optimized).

4) A vector of human operator observations in the task.

5) Observation time delay (routinely selected as $\tau_{obs} = 0.2$ s).

6) A neuromotor noise-to-signal ratio.

7) Characterization of the command signals.

For these experiments, the appropriate objective function *for each axis* was chosen to be

$$J_{\text{axis}_i} = \left[\frac{\sigma_{\epsilon_i}^2}{\sigma_{c_i}^2} + \frac{\sigma_{\dot{\delta}_i}^2}{g_i}\right] \tag{5}$$

Table 3 Configurations considered

Configuration identifyer	No. of axes	Subjective ratings	Graphical symbol
θ-*H*	1	2.5,2.5,3.0,3.0,3.0	○
θ-*M*	1	4.0,4.5,4.5,5.0,5.0	△
θ-*L*	1	6.0,6.0,6.5,7.0,8.0	▽
ϕ-*H*	1	2.5,3.0,3.0,4.0,4.0	□
ϕ-*M*	1	3.5,4.0,4.0,5.0,5.0,5.0	◇
ϕ-*L*	1	5.0,5.5,6.0,6.5	▷
β-*H*	1	3.0,3.5,3.5,3.5,3.5	◁
$\theta\phi$-*HH*	2	(2.0,3.0,3.0,3.0,3.5)[a]	○
$\theta\phi$-*HL*	2	(6.0,6.0,6.5)[a]	▷
$\theta\phi$-*ML*	2	(6.0,7.0,7.0)[a]	◁
$\theta\phi$-*LH*	2	(4.0,4.0,4.0)[a]	▽
$\theta\phi\beta$-*HHH*	3	5.5,6.0,6.0,6.0	●
$\theta\phi\beta$-*HMH*	3	5.0,5.5,6.0	▲
$\theta\phi\beta$-*HLH*	3	7.0,9.0	▼
$\theta\phi\beta$-*MHH*	3	5.5,6.5,6.5	■
$\theta\phi\beta$-*MMH*	3	7.5	◆
$\theta\phi\beta$-*MLH*	3	8.0,8.5	▶
$\theta\phi\beta$-*LHH*	3	9.0,10.0	◀
$\theta\phi\beta$-*LMH*	3	9.0	▬
$\theta\phi\beta$-*LLH*	3	8.5,9.5	▬

[a]Data considered inconsistent—not specifically used.

Table 4 Dander command signal content

Axis	Frequency (rad/s)	Unscaled amplitude
θ_c	0.367	4.80
	0.483	2.20
($\theta_{c_{max}} \approx \pm 0.75$ in.)	0.816	1.15
	1.32	1.64
ϕ_c	0.367	4.80
	0.483	5.50
($\phi_{c_{max}} \approx \pm 45$ deg)	0.816	1.44
	1.32	1.64
β_c	0.483	0.92
	0.816	0.33
($\beta_{c_{max}} \approx \pm 1.8$ units)	1.32	0.33

And for a multiaxis task, the objective function for the task was

$$J_{\text{task}} = \sum_{i}^{N_{\text{axes}}} J_{\text{axis}i} \tag{6}$$

The justification of this selection involves three considerations. The first relates to the selection of equal (unity) weighting on each $J_{\text{axis}i}$ in the definition of J_{task} in multiaxis tasks. This decision was based on the instructions given to the subjects in the experiment. They were to attempt to minimize the error in all controlled axes. That is, they were instructed that no axis was to be given preference, which would then define primary and secondary subtasks.

Second, the normalization of the mean-square error with the mean-square command deals nicely with the fact that different units and different command-signal strengths were used in the axes. This will be discussed further with regard to subjective ratings.

Finally, the interpretation of g_i requires some discussion. In exercising the optimal control model (OCM), it is often cited that g_i is selected to yield a desired neuromotor time constant τ_n in the pilots' describing function obtained from the model. [Incidentally, when the total pilot describing function Y_p is actually constructed from its consitutent elements in the OCM, the τ_n established in this fashion is canceled by a directly compensating lead. The actual estimated Y_p is then left with no $(\tau_n s + 1)^{-1}$ lag. Still, it has been convenient to adjust g_i in this fashion even though the lag will later disappear.] For the analysis to follow, the value of the desired neuromotor time constant used is either 0.1 s, *or* the τ_n that yields the lowest error (e.g., best performance), whichever is *greater*. Notice that after a τ_n is determined in the preceding fashion, this "operating point" is associated with some weight g_i in $J_{\text{axis}i}$. This value may also imply a subjective trade between performance σ_ϵ and workload $\sigma_{\dot{\delta}}$. And since pilot lead and $\sigma_{\dot{\delta}}$ are related, this procedure maximizes the possibility of relating the resulting value of J_{task} to the subjective rating of the task.

The parameters related to observation noise selected were as follows. For the experimental setup considered, and using visual perception thresholds of 0.05 deg and 0.1 deg/s of visual arc and arc rate at the pilot's eye, the dead-zone widths for the perception thresholds are $\theta = 0.03$ in., 0.05 in./s; $\phi = 1.5$ deg, 3.0 deg/s; and $\beta = 0.14$ unit, 0.28 units/s. The nominal full-attention foveal-viewing value of -20 dB was selected as the basic noise-to-signal ratio P_0 for both perceived error and error rate in each axis. And finally, for multiaxis tasks, the attention was optimized among observations for each axis, with the fractional attention f_i [see Eq. (4)] constrained to be equal for both error and error rate in each axis. This optimization was performed using the criteria that f_i were to be chosen such that J_{task} was minimized, subject to the constraint that

$$\sum_{\text{axis}} f_i = 1 \tag{7}$$

For further discussion of the attentional allocation, see Ref. 13.

The observations assumed available to the subjects were error and error rates in each axis. The displays were either integrated or considered sufficiently close together such that additional observation errors due to scanning or parafoveal viewing were neglected.

The neuromotor noise-to-signal ratio was selected to be -20 dB. In addition to neuromotor noise reflecting a source of remnant, the use of this noise has also been found to be necessary for the OCM to yield gain and phase margins appropriate for human operator modeling. For the relation between this noise and stability margins of linear-quadratic-Gaussian (LQG) controllers, the reader is referred to Ref. 14.

Finally, the command signal for each axis was modeled as low-passed white noise, using the filter

$$F_c(s) = \frac{A_c}{s^2 + 2(0.7)(0.5)s + (0.5)^2} \tag{8}$$

Note that the break frequency of 0.5 rad/s corresponds to maximum command power below 0.5 rad/s. The gain A_c was selected such that the maximum command amplitude listed in Table 4 was twice the standard deviation (2σ) of the random command generated with the previously mentioned filter.

Results of the Model Analysis

The aforementioned OCM setup data were used with a version of the PIREP computer program[13] to obtain OCM-based estimates for the pilot dynamic behavior and various system performance metrics. The model results obtained include both time- and frequency-domain quantities. The time-domain results include root-mean-square tracking error σ_ϵ, control manipulation deflection rate σ_δ, the objective function magnitude J_{task}, and the optimized attentional allocation f_i for each axis (for multiaxis tasks). The frequency-domain results include pilot describing function $Y_p(j\omega) = \delta_i/\epsilon_i(j\omega)$ and remnant $\phi_{nn}(\omega)$, along with the controlled-element transfer function in Bode form $\epsilon_i/\delta_i(j\omega)$. From this information, the crossover frequency ω_{c_i}, pilot phase compensation at crossover $\phi_p(\omega_c)$, phase margin ϕ_M, effective pilot latency τ_E, and closed-loop bandwidth may be determined. These parameters are obtained graphically as, for example, in Refs. 15 and 16. The pilot's describing function (in each axis) that is obtained from the OCM may be considered to be of the form

$$Y_p(j\omega) = \frac{e^{j\omega\tau_{\text{obs}}}}{j\omega\tau_n + 1}\,\hat{Y}_p(j\omega) \tag{9}$$

And the pilot phase compensation is then

$$\phi_p(\omega_c) = \arg\,\hat{Y}_p(j\omega_c) \tag{10}$$

The phase margin is determined from

$$\phi_M = \pi - \arg\,Y_pY_c(j\omega_c) \tag{11}$$

while effective pilot latency is

$$\tau_E = (\pi/2 - \phi_M)/\omega_c \tag{12}$$

Finally, the closed-loop bandwidth is defined as

$$\omega_{BW} = \omega\,|_{\text{closed loop phase} = -90\text{ deg}} \tag{13}$$

The key results are summarized in Tables 5–7. Table 5 lists the single-axis results. When the single-axis estimates are converted to classical forms, the results show trends of rating with increased effective latency τ_e and reduced crossover frequency ω_c, which are consistent with similar sets of vehicle dynamics considered in Refs. 1 and 17. Tables 6 and 7 summarize the two- and three-axis results, respectively. These results will be discussed further.

Since one of the fundamental effects of task interference is increased remnant, this area is the first to be discussed. Shown in Fig. 3 are the modeling results for the remnant ϕ_{nn}, normalized with mean-squared error for two cases considered. This figure does, indeed, indicate an increase in remnant at low frequencies for the two-axis task over the single axis. Note that this two-axis task involves poor dynamics laterally, with the same good dynamics in pitch as the single-axis case. As a result of the interference from difficult lateral dynamics, the attention allocated to the pitch axis reduces from 100% ($f_{\text{pitch}} = 1.0$) to 20% ($f_{\text{pitch}} = 0.2$).

One reason the controlled elements of Fig. 3 were chosen for single-axis, dual-axis comparisons, is the possibility to compare the estimation results with similar data. Reference 6 considered a two-axis case with one axis involving an unstable

Table 5 Single-axis summary

Case	$\omega_c(r/s)$	ω_{BW}	$\phi_M(\tau_e)$	ϕ_{pc}	σ_ϵ/σ_i	σ_δ/g_i	J	POR
θ_{Hi}	3.2	3.7	37°(0.289)	44.2°	0.188	0.103	0.46	2.5–3
θ_{Mid}	3.1	3.5	28.4(0.346)	42.6	0.295	0.193	0.124	4–5
θ_{Low}	3.1	3.5	25.5(0.363)	44.8	0.413	0.273	0.245	6–7
ϕ_{Hi}	3.1	3.6	37.2(0.297)	50.7	0.202	0.119	0.055	2.5–4
ϕ_{Mi}	3.1	3.5	29.5(0.335)	64.5	0.281	0.176	0.110	3.5–5
ϕ_{Low}	2.8	3.1	21.5(0.427)	64.0	0.523	0.385	0.422	5–6.5
$(\tau_n = 0.12)$[a]								
β_{Hi}	2.9	3.6	43.4(0.280)	38.9	0.234	0.125	0.071	3–3.5

[a] $\tau_n = 0.1$ s except as noted.

Table 6 Two-axis summary[a]

Case/axis	ω_c	ω_{BW}	$\phi_M(\tau_e)$	ϕ_{pc}	σ_ϵ/σ_i	σ_δ/g_i	Attentional fraction	J_{task}	POR
$\theta\phi$,HH/θ	2.75	3.3	41.5(0.308)	39.0	0.230	0.111	0.5	0.140	(2.9)
$\theta\phi$,HH/ϕ	2.7	3.3	42.2(0.308)	43.7	0.242	0.126	0.5		
$\theta\phi$,HL/θ	2.15	2.85	49.2(0.331)	33.9	0.315	0.127	0.2	0.646	(6.2)
$\theta\phi$,HL/ϕ	2.75	2.95	22.1(0.431)	62.8	0.594	0.421	0.8		
$\theta\phi$,LH/θ	3.0	3.4	26.3(0.371)	44.1	0.472	0.235	0.8	0.430	(4.0)
$\theta\phi$,LH/ϕ	2.2	2.87	51.0(0.309)	34.1	0.306	0.134	0.2		

[a] τ_n in each axis as in Table 4.

Table 7 Three-axis summary[a]

Case/axis	ω_c	ω_{BW}	$\phi_M(\tau_e)$	ϕ_{pc}	σ_ϵ/σ_i	σ_δ/g_i	Attn.	J_{task}	POR
$\theta\phi\beta$,*HHH*/θ	2.5	3.1	45.(0.314)	36.6	0.262	0.118	0.33	0.300	5.5-6
$\theta\phi\beta$,*HHH*/ϕ	2.45	3.1	46.(0.313)	39.1	0.273	0.130	0.33		
$\theta\phi\beta$,*HHH*/β	2.0	2.8	54.2(0.312)	17.2	0.330	0.126	0.33		
$\theta\phi\beta$,*HLH*/θ	1.9	2.6	53.1(0.339)	32.5	0.368	0.134	0.15	0.935	7.-9.0
$\theta\phi\beta$,*HLH*/ϕ	2.65	2.9	23.5(0.438)	61.3	0.644	0.445	0.67		
$\theta\phi\beta$,*HLH*/β	1.75	2.6	60.7(0.292)	16.9	0.389	0.140	0.18		
$\theta\phi\beta$,*LHH*/θ	2.9	3.3	26.8(0.380)	42.8	0.505	0.244	0.67	0.539	9.0-10.0
$\theta\phi\beta$,*LHH*/ϕ	1.9	2.6	56.5(0.308)	27.9	0.360	0.140	0.15		
$\theta\phi\beta$,*LHH*/β	1.63	2.6	60.2(0.319)	4.4	0.394	0.132	0.18		
$\theta\phi\beta$,*MMH*/θ	2.6	3.0	32.3(0.395)	36.0	0.430	0.165	0.40	0.631	7.5
$\theta\phi\beta$,*MMH*/ϕ	2.7	3.1	34.5(0.366)	58.5	0.420	0.186	0.40		
$\theta\phi\beta$,*MMH*/β	1.7	2.5	59.5(0.318)	7.3	0.380	0.131	0.20		
$\theta\phi\beta$,*MHH*/θ	[b]	[b]	[b]	[b]	0.370	0.211	0.48	0.426	5.5-6.5
$\theta\phi\beta$,*MHH*/ϕ	[b]	[b]	[b]	[b]	0.293	0.131	0.27		
$\theta\phi\beta$,*MHH*/β	[b]	[b]	[b]	[b]	0.349	0.138	0.25		
$\theta\phi\beta$,*HMH*/θ	[b]	[b]	[b]	[b]	0.295	0.126	0.25	0.421	5.0-6.0
$\theta\phi\beta$,*HMH*/ϕ	[b]	[b]	[b]	[b]	0.381	0.210	0.46		
$\theta\phi\beta$,*HMH*/β	[b]	[b]	[b]	[b]	0.333	0.137	0.29		
$\theta\phi\beta$,*LMH*/θ	[b]	[b]	[b]	[b]	0.533	0.322	0.54	0.859	9.0
$\theta\phi\beta$,*LMH*/ϕ	[b]	[b]	[b]	[b]	0.490	0.242	0.28		
$\theta\phi\beta$,*LMH*/β	[b]	[b]	[b]	[b]	0.388	0.140	0.18		
$\theta\phi\beta$,*MLH*/θ	[b]	[b]	[b]	[b]	0.508	0.257	0.28	1.23	8.0-8.5
$\theta\phi\beta$,*MLH*/ϕ	[b]	[b]	[b]	[b]	0.695	0.468	0.59		
$\theta\phi\beta$,*MLH*/β	[b]	[b]	[b]	[b]	0.428	0.142	0.13		
$\theta\phi\beta$,*LLH*/θ	[b]	[b]	[b]	[b]	0.682	0.386	0.39	1.74	8.5-9.5
$\theta\phi\beta$,*LLH*/ϕ	[b]	[b]	[b]	[b]	0.788	0.512	0.51		
$\theta\phi\beta$,*LLH*/β	[b]	[b]	[b]	[b]	0.472	0.143	0.10		

[a] τ_n in each axis as in Table 4. [b] Not determined.

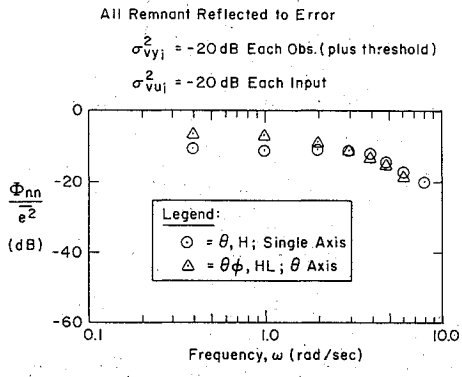

Fig. 3 Model-based error remnant spectrum task-interference effect.

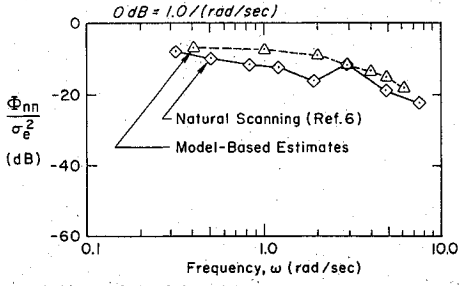

Fig. 4 Comparison of model-estimated and Ref. 6 normalized remnant spectra.

controlled element similar to the lateral dynamics for the two-axis case modeled here. Figure 4 shows that the remnant shown for the pitch axis in the two-axis task in Fig. 3 compares favorably with that from Ref. 6 for the natural-scanning case. To the extent that these remnant data from Ref. 6 are a reasonable surrogate for the Dander case, this close correspondence is compelling. However, a key result is that an *increase in remnant* due to task interference is reflected in the results from the optimal control model, consistent with the classical theory reviewed earlier.

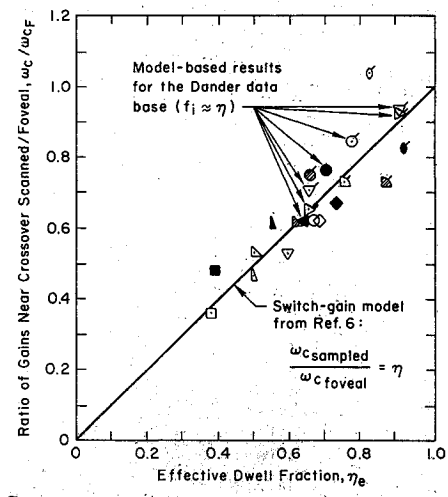

Fig. 5 Crossover regression with task interference (after Ref. 6).

Another noted effect of interference was ω_c regression. Shown in Fig. 5 are some experimental results from Ref. 6 along with some model-based results generated in this study. The ratio of crossover frequency to that for a single-axis task is plotted vs effective dwell fraction η_e defined as

$$\eta_e = \eta - \Omega(1-\eta) \tag{14}$$

where Ω = ratio of crossover gains for divided/full attention (≈ 0.566 for the Ref. 6 data), and η = actual dwell fraction. If dwell fraction is taken to approximate fractional attention f_i as defined herein (or vice versa), one can compare model-based results to those of Ref. 6. The modeling results are in general agreement with the experimental data and exhibit the same trends as expected from the theory. Therefore, we can say that the task interference effect of ω_c *regression* is also observed in the optimal control modeling results.

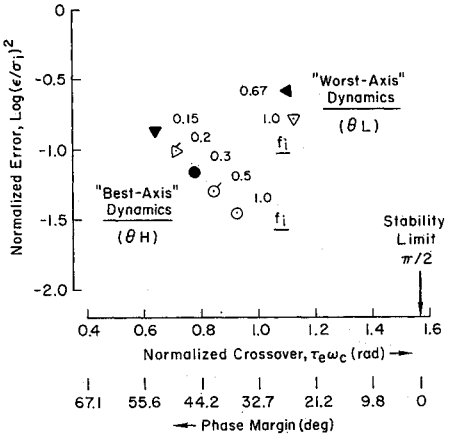

Fig. 6 Trend of optimal operating points.

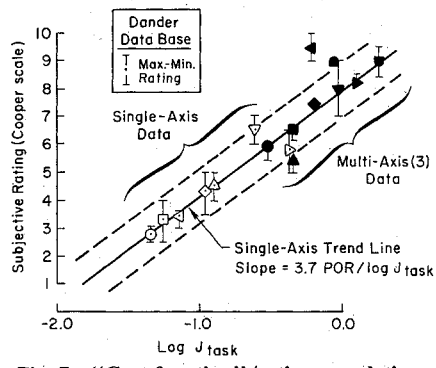

Fig. 7 "Cost function"/rating correlation.

Another comparison between the classical theory and the optimal control modeling results discussed herein is revealed in Fig. 6. The results in this figure are consistent with the parametric results shown in Fig. 2. The minima in Fig. 2 represent the optimum performance σ_ϵ for a given dwell fraction η. Again interpreting η to be analogous to fractional attention f_i, the optimal-control-model-based results for the Dander configuration in Fig. 6 corresponding to "best" dynamics, for example, are the model-based results that show trends comparable to the minimum mean-squared error points of Fig. 2. Listed alongside the data points in Fig. 6 is the fractional attention used for control of the best axis dynamics (θH) and some results for the "worst" axis dynamics (θL). Note that as fractional attention (dwell fraction) decreases for a given controlled element, (optimum) *tracking performance is degraded, ω_c regresses, and phase margin increases*—all generally consistent with the classical divided-attention theory.

Pilot Rating Estimation

Given the consistencies between full- and divided-attention behavior described previously, the next concern is the estimation of pilot workload associated with the multiaxis control tasks. This is quantified in the Dander data set by Cooper pilot ratings. It is well known (e.g., Refs. 1, 12, 17) that the subjective ratings of flying qualities provided by pilots depend on task performance and the pilot equalization needed to offset any deleterious vehicle dynamic characteristics. In tasks with a significant closed-loop tracking content these features can be reasonably represented by normalized tracking error and pilot lead equalization.

Pilot lead equalization will skew the pilot's output ("control input" in the OCM) spectrum toward higher-frequency content. Consequently, lead equalization when reflected into a component of an integral performance index will be manifest as increased control input rate. Also, the task performance in terms of mean-squared error is a natural component of a system performance metric or index. With these two facts in mind, Hess[18] suggested that the combination of error squared and pilot-output-(control input)-rate squared might be used as a metric giving indication of the subjective rating. With a particular weighting g on the control rate term, this is just the optimal control performance index in the OCM. Using the limited experimental data available, Hess[18] was able to show that a reasonable linear correlation did indeed exist between the OCM performance index J and the pilot rating, and the basis for this correlation was extended further in Ref. 19. Indeed, one reason that the present study was undertaken was the hope that this relationship could be expanded to the multiaxis situation.

To determine if the (appropriately chosen) objective function did, in fact, correlate with multiaxis and single-axis ratings, the Dander results are again considered. In the task objective functions chosen in this modeling work, the error was normalized with the variance of the command signal in the respective axis. Not only does this offset the effects of different units in the axes, but it also cancels the effect of command signal strength on the ratings.[17] Finally, with the model-based determination of g_i, the weight on control rate in the objective function, one may consider the resultant weight as "normalizing" control rate. These normalized quantities, mean-square error, and control rate are tabulated in Tables 5–7, along with J_{task}.

Shown in Fig. 7 is the correlation between J_{task}, as modeled, and the subjective ratings of the task. The correlation between J_{task} and pilot opinion rating (POR) from the single-axis results appear to hold for the multiaxis results as well. This result would seem to indicate that the ratings reflect the actual performance and workload (stick rate) in the overall task, or that the subject does not accept the fact that the performance should be worse since the task is more difficult. In other words, the subject does not accept worse performance and workload in a multiaxis task compared to single-axis results.

The results also tend to support the hypothesis that determining the weightings g_i in the manner discussed leads to appropriate relative weightings on control rate in the axis, and the relative weight between control rate and normalized error.

Conclusions

Pilot modeling estimates using the optimal control model adjusted to take into account divided attention or task interference among several control axes indicate that when the pilot must divide his attention across several control axes, the crossover frequency will be less than full-attention values, while the remnant, closed-loop system performance (error) and phase margin will be larger. These results are in agreement with classical theory and available experimental data. Finally, the objective function (optimal control performance index) used in the pilot and system behavioral modeling, when "calibrated" with single-axis correlations, shows potential for the development of subjective ratings estimates for multiaxis tasks.

Acknowledgment

This research was supported under Contract F33615-85-C-3610 from the Flight Dynamics Laboratory, Air Force Wright Aeronautical Laboratories, Wright-Patterson Air Force Base, Ohio. The contract technical monitor was Mr. Thomas Gentry.

References

[1]McRuer, D. T. and Krendel, E. S., "Mathematical Models of Human Pilot Behavior," AGARDograph 188, Jan. 1974.

[2]Bergen, A. R., "On the Statistical Design of Linear Random Sampling Systems," *Automatic and Remote Control (Proceedings of the First International Congress IFAC)*, edited by J. F. Coales, J. R. Ragazzini, and A. T. Fuller, Butterworths, London, 1961, pp. 430–436.

[3]Clement, W. F., "Random Sampling Remnant Theory Applied to Manual Control," Systems Technology, Inc., Hawthorne, CA, TM-183-A., March 1969.

[4]Jex, H. R., Allen, R. W., and Magdaleno, R. E., "Display Format Effects on Precision Tracking Performance," Aerospace Medical Research Lab., Wright-Patterson AFB, OH, AMRL-TR-71-63, Aug. 1971.

[5]McRuer, D. T., Jex, H. R., Clement, W. F., and Graham, D., "Development of a Systems Analysis Theory of Manual Control Displays," Systems Technology, Inc., TR-163-1, Oct. 1967, revised June 1968.

[6]Allen, R. W., Clement, W. F., and Jex, H. R., "Research on Display Scanning, Sampling, and Reconstruction Using Separate Main and Secondary Tracking Tasks," NASA CR-1569, July 1970.

[7]Hollister, W. M. (ed.), "Improved Guidance and Control Automation at the Man-Machine Interface," AGARD Advisory Rept. 228, Dec. 1986.

[8]McRuer, D. T., Clement, W. F., and Magdaleno, R. E., "Computer-Aided Procedure for Analyzing Man-Machine System Dynamic Interactions: Simplified Pilot-Modeling for Divided Attention Operation," Vol. II, Wright Research and Development Center, Wright-Patterson AFB, OH, WRDC-TR-89-3070, June 1989.

[9]Levison, W., Elkind, J., and Ward, J., "Studies of Multivariable Manual Control Systems: A Model of Task Interference," NASA CR-1746, May 1971.

[10]Kleinman, D., Baron, S., and Levison, W., "An Optimal Control Model of Human Behavior," *Automatica*, Vol. 6, 1970, pp. 357–369.

[11]Dander, V., "An Evaluation of Four Methods for Converting Single Axis Pilot Ratings to Multi-Axis Pilot Ratings Using Fixed Base Simulation Data," M.S. Thesis, Air Force Inst. of Technology, Wright-Patterson AFB, OH, GE/EE/62-4, Dec. 1962.

[12]Ashkenas, I. L., Hoh, R. H., and Craig, S., "Recommended Revisions to Selected Portions of MIL-F-8785B (ASG) and Background Data," Air Force Flight Dynamics Lab., Wright-Patterson AFB, OH, AFFDL-TR-73-76, Aug. 1973.

[13]Curry, R., Hoffman, W., and Young, L., "Pilot Modeling for Manned Simulation," Air Force Flight Dynamics Lab., Wright-Patterson AFB, OH, TR-76-124, Vols. 1 and 2, Dec. 1976.

[14]Doyle, J. and Stein, G., "Robustness with Observers," *IEEE Transactions on Automatic Control*, Aug. 1979.

[15]Bacon, B. and Schmidt, D., "A Modern Control Approach to Pilot/Vehicle Analysis and the Neal-Smith Criteria," *Journal of Guidance, Control, and Dynamics*, Vol. 19, Sept.–Oct., 1983, pp. 339–347.

[16]Anderson, M. R. and Schmidt, D. K., "Closed-Loop Pilot Vehicle Analysis of the Approach and Landing Task," *Journal of Guidance, Control, and Dynamics,* Vol. 10, March–April 1987, pp. 187–194.

[17]McDonnell, J., "Pilot Rating Techniques for the Estimation and Evaluation of Handling Qualities," Air Force Flight Dynamics Lab., Wright-Patterson AFB, OH, TR-68-76, May 1968.

[18]Hess, R., "Prediction of Pilot Opinion Ratings Using an Optimal Pilot Model," *Human Factors*, Vol. 19, No. 5, 1977.

[19]Schmidt, D. K., "On the Use of the OCM Objective Function as a Pilot Rating Metric," 17th Annual Conference on Manual Control, UCLA, June, 1981.